

Document downloaded from:

<http://hdl.handle.net/10251/100042>

This paper must be cited as:

Tur Valiente, M.; Fuenmayor Fernández, F.; J.J. Ródenas; Giner Maravilla, E. (2003). 3D analysis of the influence of specimen dimensions on fretting stresses. *Finite Elements in Analysis and Design*. 39(10):933-949. doi:10.1016/S0168-874X(02)00139-7



The final publication is available at

[https://doi.org/10.1016/S0168-874X\(02\)00139-7](https://doi.org/10.1016/S0168-874X(02)00139-7)

Copyright Elsevier

Additional Information

‘3D analysis of the influence of specimen dimensions on fretting stresses’

M. Tur, J. Fuenmayor, J. J. Ródenas, E. Giner

Departamento de Ingeniería Mecánica y de Materiales

Universidad Politécnica de Valencia

Camino de Vera s/n, 46022, Valencia (Spain)

e-mail: matuva@mcm.upv.es

Abstract

In this paper, the contact conditions and stresses that arise in a fretting test have been analysed by means of a three-dimensional finite element model of the contact between a sphere and a flat surface. An h -adaptive process, based on element subdivision, has been used in order to obtain a low discretization error at a reasonable computational cost. The influence of finite dimensions of the specimen in the stress fields has been evaluated. The results have been compared with the classical Cattaneo-Mindlin solution.

Key words: fretting; spherical contact; discretization error; h -adaptivity

1. Introduction

In engineering, the term fretting is used to describe the process of damage produced at the interface of two bodies in contact subjected to some relative oscillatory slip movement of small amplitude. As a result of such a phenomenon a number of cracks could be initiated in the contact zone. These cracks may produce surface degradation by generation and subdivision of small debris or may grow and expand inside one of the bodies eventually producing fracture. This process appears in many mechanical systems, such as bolted and riveted joints, shrink fitted shaft connections, blade connections, medical implants, etc.

A number of test devices, where the contact pads (with spherical, cylindrical or flat geometry) slip on the specimen under consideration, have been proposed in order to

study the fretting problem. According to Hills and Nowell [1], tests carried out with spherical pads possess some advantages compared with two dimensional contacts. The advantages are related to corner effects that do not appear in 3D spherical contact. Therefore, during the last few years, the number of devices developed to carry out this kind of test has increased.

Figure 1 schematically shows the fretting test analysed in this paper. Two zones of contact are generated on a flat specimen loaded with a constant tension T (creating a bulk stress) by means of the application of a constant force P on two spherical fretting pads. An alternating tangential load Q is applied after this normal load. Usually, the tangential load $|Q|$ is lower than μP , being μ the friction coefficient, so both a slip zone and a stick zone appear in the contact area. In the analytical model, the contact area and the stick zone are circular and their radii are a and c respectively [2]. The stress field near the contact zone is variable, multiaxial and non-proportional [3].

Various criteria have been proposed during the last years (see for example [4], [5], [6]) in order to evaluate initiation and growing of cracks generated in the contact area. The use of these models requires the evaluation of the stress state in the vicinity of the contact. For spherical contact problems this is usually achieved using analytical or semi-analytical methods. The first studies related to spherical bodies in contact subjected to normal and tangential loads were carried out independently by Cattaneo [1] and Mindlin [8], [9]. These authors considered the bodies in contact as infinite half-spaces. Hamilton and Goodman [10] obtained the stress field inside the bodies loaded with a hertzian distribution of normal and tangential contact stresses on the surface. Hamilton [11] and Sackfield and Hills [12] extended the previous work obtaining a formulation that is easier to process. Using these previous works Domínguez [3] calculated the evolution of the stresses in a fretting fatigue test cycle. As Domínguez shows, the solution obtained

is only approximate because of the finite dimensions of the specimen, tangential contact stress perpendicular to the tangential load, and some other aspects such as surface wear, surface roughness, etc., are not considered.

Munisamy *et al.*[13] studied the tangential traction in a direction perpendicular to the tangential load Q for sphere-flat contact problems using a semi analytical model based on influence coefficients. The effects of finite dimensions of the specimen were studied also by Nowell and Hills in [14] (variation of contact conditions and stresses) and [8] (internal stress field) in the case of 2D cylinder-flat contact.

A number of finite element models of fretting tests have been recently developed. Most of them are bidimensional analyses of cylindrical contact problems. For example, McVeigh and Farris [16] evaluated the influence of the bulk stress on the contact pressure for this kind of problem. Iyer and Mall [17] used the numerical solution to estimate fretting fatigue life. Tsai and Mall [18] incorporated elastoplastic behaviour in the material in order to obtain the evolution of stress and strains during a fretting fatigue test. In 3D contact problems using spherical pads, Giannakopoulos and Suresh [19] used a bidimensional model and a trigonometrical expansion of the displacement field to simulate the real three dimensional problem. This approximation leads to a reduction in the number of degrees of freedom necessary to obtain accurate finite element solutions. However, the effect of specimen width and bulk stress cannot be appropriately computed.

In this paper, the influence of finite dimensions of the specimen (in particular, thickness and width) in three dimensional spherical contact problems on the contact conditions and stress distribution have been analysed. The study is restricted to cases without bulk stress ($T = 0$). The evolution of contact pressure and stress field inside the specimen for different values of specimen width and thickness has been evaluated. A 3D finite

element model has been defined in order to achieve this objective. An h -adaptive process of mesh refinement has been developed ([16], [21]), with the aim of obtaining accurate solutions with a controlled discretization error, and a reasonable computational time. The finite element solution has been compared with an analytical solution in order to estimate the degree of approximation inherent in the models.

2. Finite element model

A finite element analysis of the geometrical model shown in figure 2 has been carried out to obtain the stress distribution in the specimen when using spherical fretting pads. The fretting pad consists of a modified cylinder whose lower end (in contact with the specimen) is spherical. The specimen dimension L and pad dimensions r and H are chosen to be greater than 10 times the characteristic contact size. Therefore they have a negligible influence on the stress field near the contact area. The radius of the spherical surface (R), is 50 times larger than the characteristic contact radius a .

The problem has two symmetry planes: the XY plane and the $y = -b$ plane, so the appropriate boundary symmetry conditions have been imposed. Furthermore, some restriction on the displacement of nodes located on the shaded surfaces are imposed in order to apply the other boundary conditions. Displacements in directions X , Y and Z of all nodes located on the top surface ($y = h$) of the spherical pad are forced to be identical to those of the node where the normal load P is applied (co-ordinates $x = z = 0$, $y = h$). Analogously, load Q is applied to the specimen on surface $x = L$. By means of these restrictions the transmission of the normal and tangential loads is correctly achieved. Provided the distance between the top surface and the contact zone is large enough, the applied restrictions do not affect the stress distribution near the contact. The boundary conditions minimize the rotation of the spherical pad due to the friction force. The

problem of excessive rotation of the pad appears in some finite element models in the reviewed literature where the fretting pad is constrained using low stiffness elements.

Loads have been applied in two steps in order to solve the finite element problem. In the first step, the normal load P is applied while displacements in X direction of nodes on Y axis are restricted in order to avoid rigid body motion. Afterwards, these restrictions are eliminated and the tangential load Q is applied. The value of this force should be kept under the value necessary to produce global sliding ($Q < \mu P$). In this second step, displacement in X direction of the node located in $x = z = 0, y = h$ is restricted. As the contact problem is non-linear, loads must be gradually increased in small increments. These load increments must be sufficiently small, otherwise the correct normal and tangential pressure distribution in the contact zone will not be obtained.

The finite element commercial code ABAQUS [21] has been used. This program uses the concept of master surfaces and slave nodes to define the contact between bodies. Slave nodes are chosen to be those nodes in the specimen that may come into contact with the spherical pad. The master surface has been defined as the spherical surface of the fretting pad. Contact conditions are imposed using the Lagrange multiplier method. The h -adaptive mesh refinement process used [21] is based on element subdivision. The subdivision process is based on the error indication given by the Zienkiewicz-Zhu error estimator [23]. Hexahedral elements are utilized in the FE model.

The first mesh of the sequence is directly created using the ABAQUS mesh generator. Therefore, no elements are subdivided in this mesh. An external program computes the discretization error from the finite element solution. From this calculation, the program determines which elements should be divided (ie. a new mesh is generated) in order to achieve a selected reduction of the error. The process is repeated until the specified global error is achieved. Displacement field continuity between adjacent elements with

different degree of refinement is guaranteed using multipoint constraints (MPC's). A sequence of meshes obtained using this process is shown in figure 3. In the sequence shown, the global error in energy norm for each mesh is half of the error for the previous mesh.

In all the finite element analyses, 20-node quadratic element meshes with standard integration in 3x3x3 Gauss points have been used. Elements used in the contact area are 21-node special elements [24]. A 2% global error in energy norm has been defined as the target error for all the analyses performed.

A number of analyses have been carried out for different values of the specimen semi-width d and semi-thickness b . The stress field distribution in the contact zone and inside the specimen has been studied. Sphere dimensions are the same for all the analyses. The material considered is aluminium Al 7075-T6 with Young modulus $E = 71.7$ MPa and Poisson ratio $\nu = 0.33$. A Coulomb friction model has been used in the simulation of the contact with a friction coefficient $\mu = 1.2$, which coincides with some experimental data of real fretting tests using spherical pads and the same material ([4], [5]).

3. Comparison with analytical solution

A comparison of the analytical solution for the spherical contact problem with the results obtained with the finite element model has allowed us to validate the model. For comparison purposes dimensions b and d of the specimen were chosen to be larger than 10 times the characteristic contact area size, a_∞ (radius of the contact area), in order to allow the specimen to be represented as an infinite half-space. From now onwards, magnitudes with infinite subscript refer to spherical contact problem between two bodies behaving as infinite half-spaces.

The analytical solution is based on the work carried out by Cattaneo [1] and Mindlin [9], who studied some spherical contact problems with both, normal and tangential loads. Justification of the following results can be found in [2].

When a normal load P is applied, the pressure distribution in the contact zone, according to Hertz theory, is given by:

$$p(r) = P_{0\infty} \sqrt{1 - \left(\frac{r}{a_\infty}\right)^2} \quad r \leq a_\infty \quad \text{Equation 1}$$

where $P_{0\infty}$ is the maximum value of the normal pressure and can be obtained from the following equation:

$$P_{0\infty} = \frac{3P}{2\pi a_\infty^2} \quad \text{Equation 2}$$

a_∞ is the radius of the contact area which depends on the load P and the radius R of the spherical pad as:

$$a_\infty = \sqrt[3]{\frac{1-\nu^2}{E} \frac{3RP}{4}} \quad \text{Equation 3}$$

When a monotonically increasing tangential load $Q < \mu P$ is added, the contact area is divided into a stick zone and a slip zone. The analytical solution of this problem is only approximate because the slip (and therefore the shear traction) in a direction perpendicular to the applied tangential load (Z direction) are neglected. Under this assumption, the stick zone is circular and its radius can be obtained using Q from

$$c_\infty = a_\infty \sqrt[3]{1 - \frac{Q}{\mu P}} \quad \text{Equation 4}$$

The shear traction distribution in the contact zone in X direction, q_x , is given by the following equation

$$\begin{aligned}
q_x(r) &= \mu p(r) = \mu P_{0-\infty} \sqrt{1 - \left(\frac{r}{a_\infty}\right)^2} & c_\infty \leq r \leq a_\infty \\
q_x(r) &= \mu P_{0-\infty} \left(\sqrt{1 - \left(\frac{r}{a_\infty}\right)^2} - \frac{c_\infty}{a_\infty} \sqrt{1 - \left(\frac{r}{c_\infty}\right)^2} \right) & r \leq c_\infty
\end{aligned}$$

Equation 5

Hamilton and Goodman [10] obtained the stress distribution inside an infinite half-space, assuming a hertzian contact stresses distribution. This solution has been compared with the finite element results.

The case in which only the normal load is applied is studied first. Figure 4 a) shows the normalised finite element von Mises stress distribution, $\sigma_{eq} / P_{0\infty}$, in the XY plane for this case of load. Figure 4 b) plots the differences in % of $P_{0\infty}$ between the finite element solution and the analytical model. As shown in this figure the finite element results precisely match the analytical solution. The maximum differences between the two models are about 2 % of $P_{0\infty}$.

When the tangential load is applied, the analytical solution is only an approximate one because in the analytical solution transverse slip (Z direction) is considered negligible compared to that produced in X direction. Figures 5 and 6 compare the stress distribution σ_x and τ_{xy} , respectively along the line $y = z = 0$ in the vicinity of the contact area for different values of the tangential load, Q . Good agreement is observed between the finite element results and the analytical solution for this stress component.

Differences between the finite element results and the analytical solution are found in the contact area when tangential stress τ_{yz} is considered. In figure 7 the normalised finite element tangential stress τ_{yz} in the specimen surface is presented. The external circle in figure 7 corresponds to the theoretical contact area and the internal circle the theoretical boundary between adhesion and slip zones. Results in this figure correspond to a

tangential load $Q = 0.8\mu P$ ($c = 0.585a_\infty$) and coincide with those obtained by [13] using a numerical method based on influence coefficients. This is also in agreement with the results exposed by [25], who show that these stresses are about 5% of $P_{0\infty}$. Lastly, the influence of the tangential stress τ_{yz} on the stress distribution inside the specimen has been analysed. The main differences are apparent when studying results in the XY plane. It has been found that the equivalent von Mises stresses obtained by the FE analysis beneath the slip zone are about 3% greater than those predicted by the analytical model.

4. Normal load: Influence of finite dimensions

In this section, the influence of the specimen dimensions (width and thickness) when only the normal load P is applied has been studied. A set of finite element analyses has been carried out with different values of the specimen semi-thickness, b , keeping the other dimensions, L , r , H and d , much greater (more than 10 times) than the characteristic contact size a_∞ .

The effect of the thickness reduction is the variation of the contact conditions and stresses. However, the shape of the contact area remains circular because the problem is still axi-symmetric.

Figure 8 shows the normalised normal pressure $p/P_{0\infty}$ and shear traction in X direction $q_x/P_{0\infty}$ along the X axis for different values of the specimen semi-thickness b . Plots without markers represent analytical calculations and the other plots correspond to finite element results. As the specimen semi-thickness is reduced, the maximum value of the normal pressure P_0 increases and this distribution is no longer of hertzian type. For very small values of the specimen thickness, the contact pressure distribution tends to that obtained for the case of two spheres (with radius R) in contact. In this situation, the contact becomes hertzian again as shown in figure 8. When the contact pressure is not

hertzian, an axisymmetrical distribution of tangential stresses appears in the contact area. The maximum value of these tangential stresses is about 20 % of the maximum contact pressure ($P_{0\infty}$) for a specimen semi-thickness b of about $0.3 a_{\infty}$. Figure 9 summarizes these results. The evolution of the normalised maximum contact pressure ($P_0/P_{0\infty}$) and maximum shear traction ($q_0/P_{0\infty}$) with specimen semi-thickness is plotted. The thickness influence becomes important for specimen semi-thickness lower than twice the characteristic size of the contact area a_{∞} .

Also, a variation of the contact area size a is noticed in this analysis. In figure 10 the variation of this contact size a with the specimen thickness is presented (case when tangential load $Q = 0$). The variation of the stick zone c size with specimen dimensions when $Q \neq 0$ (also shown in figure 10) will be explained in the next section. When the semi-thickness is greater than 3 times a_{∞} , the size of the contact area given by the finite element analysis is virtually the same as that for an infinite half space. On the other hand, when the thickness tends to 0 , the size of the contact area approximates that of two spheres in contact.

The values of P_0 (figure 9) and a (figure 10) could be used to obtain the stress distribution in a fretting test for a given thickness value using equations 1 and 2. In such a case, the solution would not be exact due to two factors: the tangential stresses are assumed to be zero, and the error associated with the assumption of the normal pressure as a distribution of hertzian type.

An effect of the thickness reduction is the concentration of stresses inside the specimen. As a result of this stress redistribution the maximum value of the equivalent von Mises stress increases. The point where this maximum value is obtained is approximately located at coordinates $x = z = 0, y = -0.5a_{\infty}$, for $b > 0.5a_{\infty}$. For small thickness values this point is located at $x = z = 0, y = -b$. Figure 11 shows the effect of the specimen

thickness on the evolution of the normalized maximum von Mises equivalent stress (case when $Q = 0$). There are also other plots for $Q \neq 0$ that will be commented in the next section. For $b > 0.4a_\infty$ the maximum value of the equivalent von Mises stress diminishes as the thickness is increased. When the specimen thickness is very small, the stress state inside the specimen approaches that obtained on the surface of the pads when the contact problem involves two spheres of the same radius. This value has been used in figure 11 to obtain the point for $b = 0$.

After this first analysis the specimen dimension b is kept constant (larger than 10 times the characteristic size a_∞) and the influence of specimen width d is analyzed. Only values of $d > 1.5a_\infty$ have been considered in this analysis. The effect of d on the stress state when only the normal load is applied is very small. Although in this situation the problem under consideration is not axisymmetric, the only differences between the finite element model and the analytical solution (considering infinite half spaces) appear for specimen width d of about $1.5a_\infty$ for the range analyzed. An increase of the maximum normal pressure is noticed in this situation. Small tangential stresses in the Z direction also appear, although differences with the referred analytical solution can be neglected. The contact area becomes elliptical, increasing its size along the X direction and decreasing along the Z direction although this effect is also very small.

5. Influence of finite dimensions: Tangential load

The influence of the specimen dimensions b and d on the stress distribution when a tangential load $|Q| < \mu P$ is applied in conjunction with the normal load has been analysed in this section. Figure 12 a) shows the contact pressure distribution along X -axis when the value of the tangential load is close to producing global sliding of the surfaces in contact ($Q = 0.99 \mu P$) for different values of the specimen semi-thickness.

Figure 12 b) shows the tangential shear traction q_x along the same line. As can be observed in this figure, the normal pressure, when the specimen thickness is reduced, differs from that obtained for the case $Q = 0$ (figure 8). The reason for these differences is that for very small values of semi-thickness b , the behaviour of the specimen is less compliant than that for the half space and, therefore, there exists a coupling between normal and tangential contact stresses. This coupling is similar to that obtained when the problem of two bodies in contact having different elastic properties is studied [24]. In figure 12 a) it is observed the effect of tangential stress (figure 12 b)) on the shape of the normal pressure distribution.

The changes produced in the contact conditions when the tangential load is applied are shown schematically in figure 13. The contact area remains approximately circular and its size does not depend on Q , but it is displaced towards the direction of the applied tangential force Q in the sphere (figure 13) as the specimen thickness is reduced (see also figure 12 a)). The shape of the adhesion zone remains approximately circular in all cases. An eccentricity e of this adhesion zone with respect to the contact area may appear.

For small values of specimen thickness, the shear traction distribution on the surface q_x produces a different displacement in the Y direction of points in the sphere and in the specimen. In the limit when the thickness b tends to 0 , the problem would be analogous to a sphere in contact with a body that would be rigid in the Y direction. As a result of this behaviour, points in the sphere located near B (see figure 13) will leave the contact area and points near A' will become into contact. At the same time, the maximum value of the contact pressure will displace towards point A as could be observed in figure 12 a).

This ‘stress concentration’, associated with the reduction of the specimen thickness, will cause the point with the maximum value of the von Mises stress on the surface to move towards point A (for Q values near μP). This can be observed in figure 14, where the von Mises stress distribution on the specimen surface is shown for two different values of the specimen thickness, for $Q = 0.9\mu P$. Figure 14 a) corresponds to $b = 1.25 a_\infty$ and the maximum von Mises stress appears at a point with between the end of the stick zone and the point B. The semi-thickness in figure 14 b) is $b = 0.2 a_\infty$ and the maximum von Mises stress appears in a point between A’ and the end of stick zone. The evolution of maximum value of von Mises stress (inside the specimen) with the specimen semi-thickness is presented in figure 11 for different values of the tangential load Q .

The size of the adhesion zone c , depends on the tangential load and the specimen thickness. From figure 9 the size of the adhesion zone can be obtained for different values of the tangential load Q and the specimen semi-thickness b . For a given value of the tangential load, the size of the adhesion zone, c , is reduced as the thickness is reduced. This behaviour is similar to that of the contact area size a .

The eccentricity of the stick zone with respect to the contact area could be due to two different factors. The first one is the existence of the tangential shear traction q_x in the case when the only load applied is the normal load P , due to the different compliance of the bodies. The eccentricity of the stick zone rises with increasing values of these tangential stresses. The second one is the bulk stress produced by the transmission of the tangential load Q in the specimen (this factor has to be taken into account only for those cases where this bulk stress cannot be neglected when compared to P_θ).

The influence of the specimen semi-width d has also been studied for cases where d is greater than 1.5 times the size of the contact area. The only noticeable effect of this parameter on the stress distribution can be found when studying the stresses along the

Z-axis. Figure 15 shows the components σ_z and τ_{zy} for $b = 1.5a_\infty$ and the results obtained by means of the analytical solution. As the exact solution must be zero on the boundary of the body ($z = 1.5a_\infty$), the stresses are re-distributed in order to account for this restriction. Stress distribution in the XY -symmetry plane is almost similar to the half space solution for the semi-width values considered. The differences in the von Mises stresses are below 3%.

6. Conclusions

A three-dimensional finite element model of a fretting test using spherical pads has been developed in order to study the influence of specimen dimensions on the stress field near the contact area. An h -adaptive mesh refinement procedure has been applied to obtain accurate finite element solutions at a reasonable computational cost.

For the case where only a normal load is applied, a reduction of the specimen thickness increases both the maximum contact pressure and the equivalent von Mises maximum stress inside the specimen. A reduction of the contact size area is also observed. The specimen width has no noticeable effect for values greater than 1.5 the characteristic contact area size.

When the tangential load is applied together with the normal load, the reduction of the specimen thickness produces the displacement of the contact area towards the direction opposite to the applied tangential load Q (applied in the specimen). The contact pressure distribution is also modified due to the coupling between normal and tangential stresses produced by the different compliance of the spherical pad and the specimen.

The distribution of the stress field near the contact area, both on the surface and inside the specimen, has been obtained. The analysis showed that even in the case where the

specimen and pad dimensions are only 3 times greater than the characteristic contact size, the finite element results precisely match those obtained for the contact of two infinite half spaces. This fact allows for a considerable reduction of the number of degrees of freedom of the finite element model, which is of great importance for the study of three-dimensional contact problems.

7. Acknowledgement

The authors wish to thank the financial support received from CICYT by means of the project PB97-0696-C02-02.

8. Bibliography

- [1] D. A. Hills, D. Nowell, A Critical Analysis of Fretting Fatigue Experiments, Fretting Fatigue, ESIS 18 (Edited by R. B. Waterhouse and T.C. Lindley) , Mechanical Engineering Publications, London, (1994), 171-182.
- [2] D. A. Hills, D. Nowell, Mechanics of fretting fatigue, Kluwer Academic Publishers, (1994).
- [3] J. Domínguez, Cyclic variations in friction forces and contact stresses during fretting fatigue, Wear, 218, (1998), 43-53.
- [4] B. U. Wittkowsky, P. R. Birch, J. Domínguez, S. Suresh, An experimental investigation of fretting fatigue with spherical contact in 7075-T6 aluminium alloy, Fretting fatigue: Current technology and practices, ASTM STP 1367, D. W. Hoepfner, V. Chandrasekaran, C.B. Elliot, Eds. American Society for Testing and Materials, (1999).

- [5] V. Lamacq, M.C. Dubourg, L. Vincent, Crack path prediction under fretting fatigue – a theoretical and experimental approach, *Journal of Tribology*, 118, (1996), 711-720.
- [6] C. Petiot, L. Vincent, K. Dang Van, N. Maouche, J. Foulquier, B. Journet, An analysis of fretting-fatigue failure combined with numerical calculations to predict crack nucleation, *Wear*, 181-183, (1995), 101-111.
- [7] C. Cattaneo, Sul contatto di due corpi elastici: distribuzione locale degli sforzi, *Reconditi dell'Accademia Nazionale dei Lincei*, 27, (1939).
- [8] R.D. Mindlin, H. Deresiewicz, Elastic spheres in contact under varying oblique forces, *Journal of Applied Mechanics*, 75, (1953), 327-344.
- [9] R.D. Mindlin, Compliance of elastic bodies in contact, *Journal of Applied Mechanics*, (1949), 259-268.
- [10] G.M. Hamilton, L. E. Goodman, The Stress Field Created by a Circular Sliding Contact, *Journal of Applied Mechanics*, 33, (1966), 371-376.
- [11] G.M. Hamilton, Explicit Equations for the Stresses Beneath a Sliding Spherical Contact, *Proc. Instn. Mech. Engrs.*, 197 C, (1982), 53-59.
- [12] A. Sackfield, D.A. Hills, A note on the Hertz contact problem: a correlation of standard formulae, *Journal of Strain Analysis*, 18 –3, (1983), 195-197.
- [13] R. L. Munisamy, D.A. Hills, D. Nowell. Static Axisymmetric Hertzian Contacts Subject to Shearing Forces. *Journal of Applied Mechanics*, 61, (1994), 278-283
- [14] D. Nowell, D.A. Hills. Contact Problems Incorporating Elastic Layers. *International Journal of Solids and Structures*. 24-1, (1998), 105-115.

- [15] L.J. Fellows, D. Nowell, D.A. Hills, Contact Stresses in a Moderately Thin Strip (with particular reference to fretting experiments), *Wear*, 185, (1995), 235-238.
- [16] P. A. McVeigh, T.N. Farris, Finite Element Analysis of Fretting Stresses, *Journal of Tribology*, 119, (1997), 797-801.
- [17] K. Iyer, Peak contact pressure, cyclic stress amplitudes, contact semi-width and slip amplitude: relative effects on fretting fatigue life, 2001, *International Journal of Fatigue*, 23, 193-206.
- [18] C.T. Tsai, Shankar Mall, Elasto-plastic finite element analysis of fretting stresses in pre-stressed strip in contact with cylindrical pad, *Finite elements in analysis and design*, 36, (2000), 171-187.
- [19] A.E. Giannakopoulos, S. Suresh, A three-dimensional analysis of fretting fatigue, *Acta Materialia*, 46-1, (1997), 177-192.
- [20] F.J. Fuenmayor, J.L. Oliver, Criteria to achieve nearly optimal meshes in the h -adaptive finite element method, *Int. J. Num. Methods in Engineering*, 39, (1996), 4039-4061.
- [21] J.J. Ródenas, M. Tur, J.E. Tarancón, F. Fuenmayor, H-adaptatividad de Elementos Finitos en Refinamiento por Subdivisión de Malla, *Congreso Nacional de Ingeniería Mecánica III*, (2000), 1652-1658.
- [22] ABAQUS/Standard User's Manual, version 5.8, Hibbit, Karlsson & Sorensen, Pawtucket R.I., (1996).
- [23] O.C. Zienkiewicz, J.Z. Zhu. A simple error estimator and adaptive procedure for practical engineering analysis, *Int. J. Num. Methods in Engineering*, 24, (1987), 337-357.

- [24] R. Buczkowski, 21-node hexahedral isoparametric element for analysis of contact problems, *Commun. Numer. Meth. Engng.*, 14, (1998) , 681-692.
- [25] C. Navarro, J. Domínguez, Contact conditions and stresses induced during fretting fatigue, *Computational Methods in Contact Mechanics IV*, (1999), 453-462.
- [26] T.N. Farris, Mechanics of Fretting Fatigue Tests of Contacting Dissimilar Elastic Bodies, *Tribology Transactions*, 35-2, (1992), 346-352.

FIGURE CAPTIONS

Figure 1.- Schema of loads applied during a fretting experiment using spherical pads

Figure 2.- Geometrical model of the fretting test using spherical pads

Figure 3.- Example of h-adaptive mesh refinement sequence

Figure 4.- Normalised von Mises stress distribution on the XY plane of the specimen when only the normal load P is applied. a) FE solution, b) Differences between FE and analytical solution

Figure 5.- Normal stress σ_x along X axis for different tangential load Q values

Figure 6.- Tangential stress τ_{xy} along X axis for different values of tangential load Q

Figure 7.- Finite element tangential stress distribution τ_{yz} in the contact zone. $Q = 0.9\mu P$

Figure 8.- Contact pressure along X axis for different values of specimen thickness. $Q = 0$

Figure 9.- Evolution of normalised maximum normal and tangential stresses in the contact with the specimen thickness

Figure 10.- Size of the contact area and adhesion zone versus specimen thickness

Figure 11.- Maximum equivalent von Mises stress vs. the specimen thickness for different values of the tangential load

Figure 12.- a) Contact pressure distribution along X-axis for different values of specimen thickness. b) Tangential stress distribution in the contact zone

Figure 13.- Changes in contact conditions when the tangential load is applied

Figure 14.- Equivalent von Mises stress in the contact area with tangential load $Q = 0.9\mu P$

a) $b = 1.25a_\infty$ b) $b = 0.2a_\infty$

Figure 15.- Stresses σ_z and τ_{yz} for $z=1.5a_\infty$ and half-space along Z axis. Tangential load $Q = 0.99 \bullet P_0$

Figure 1

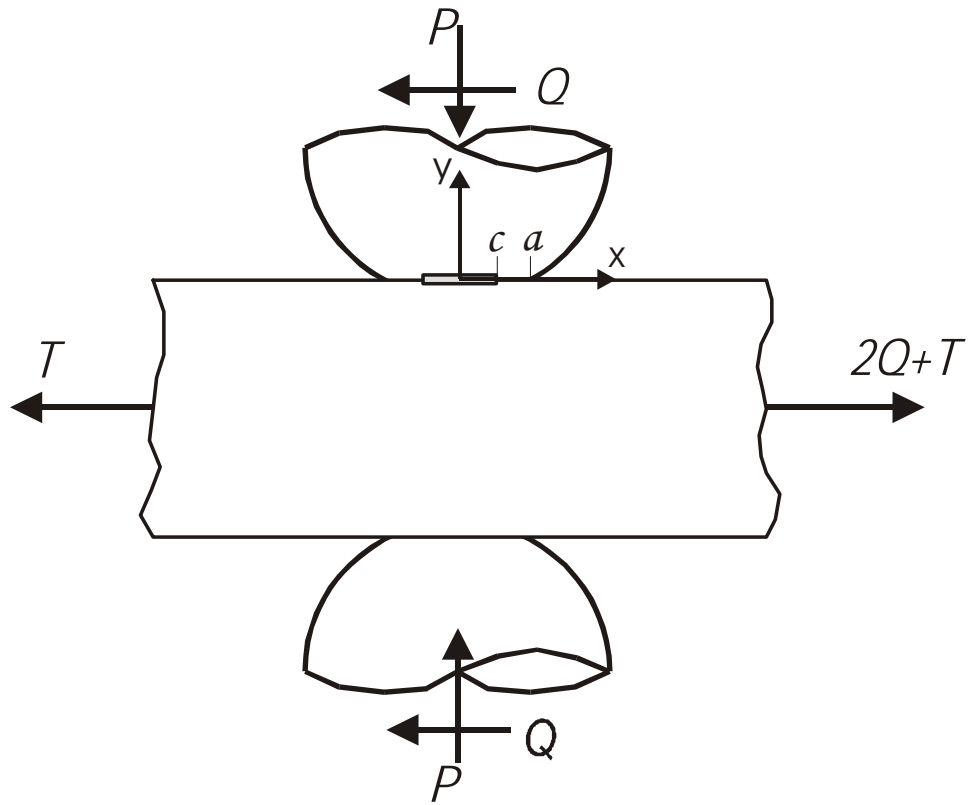


Figure 2

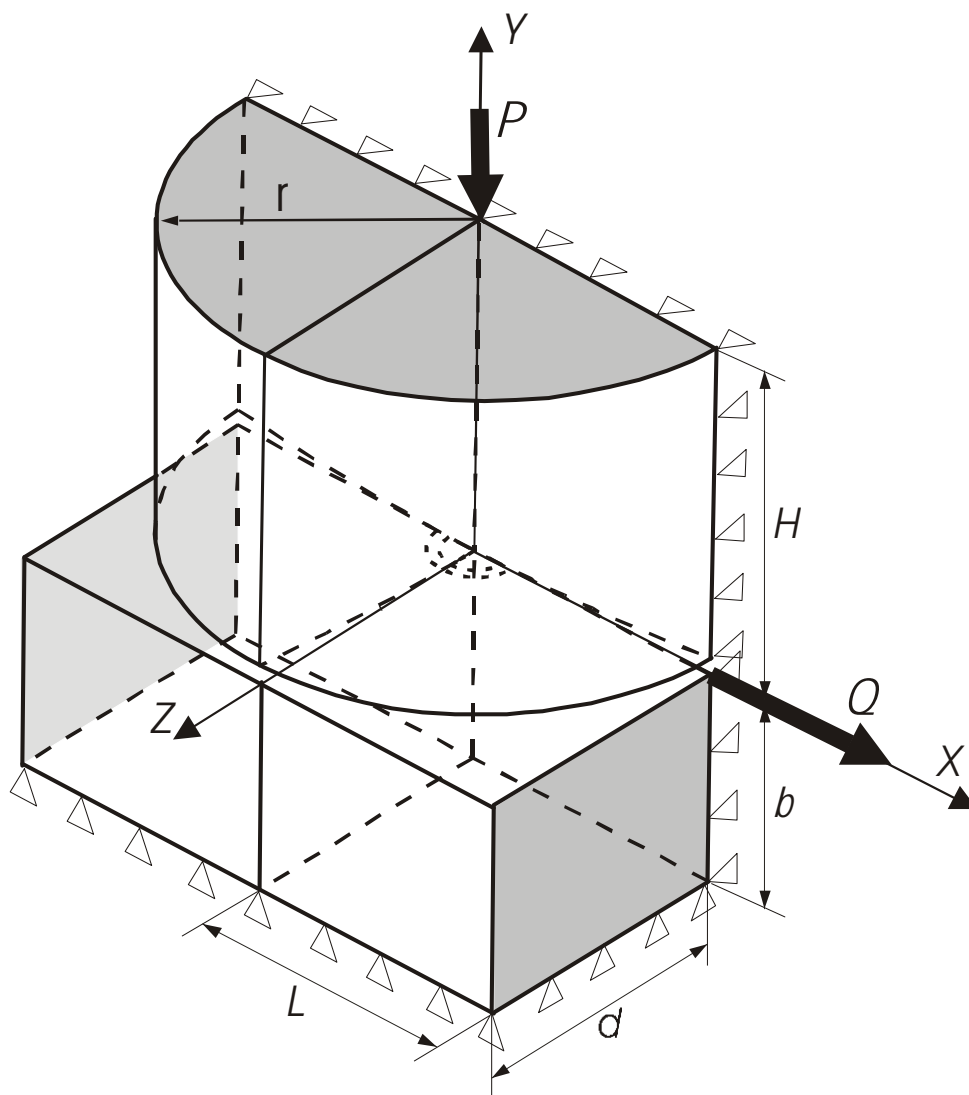


Figure 3

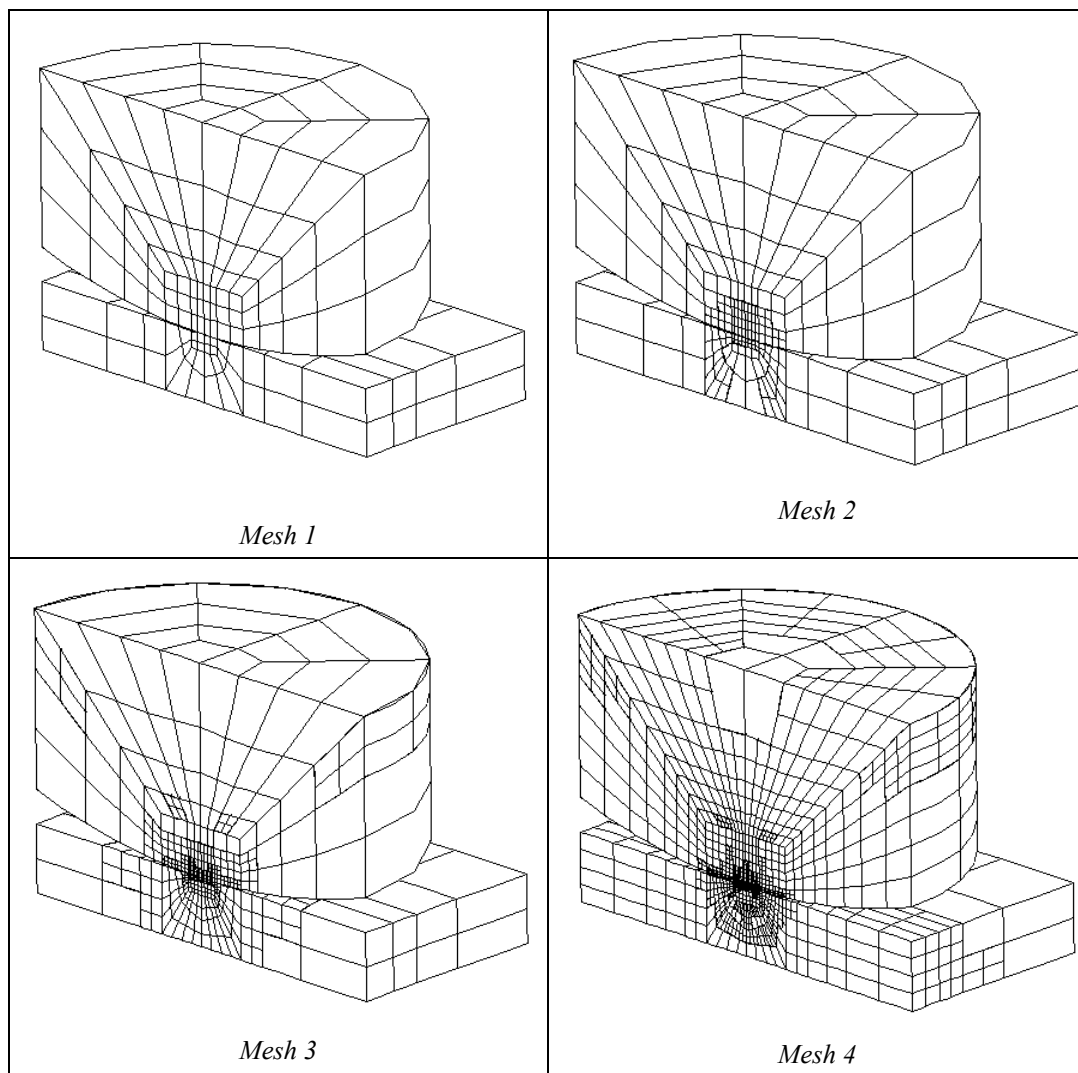
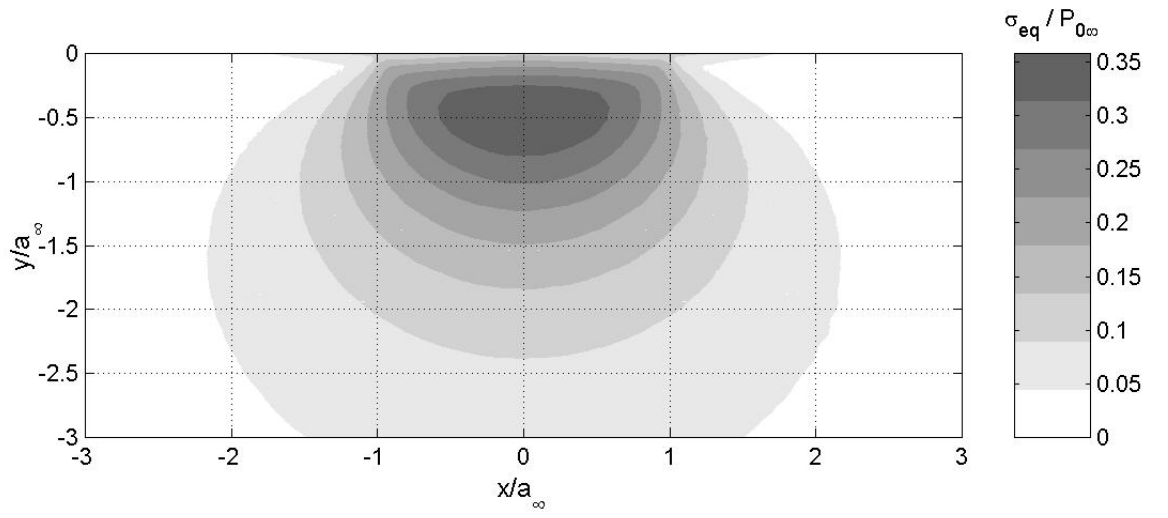
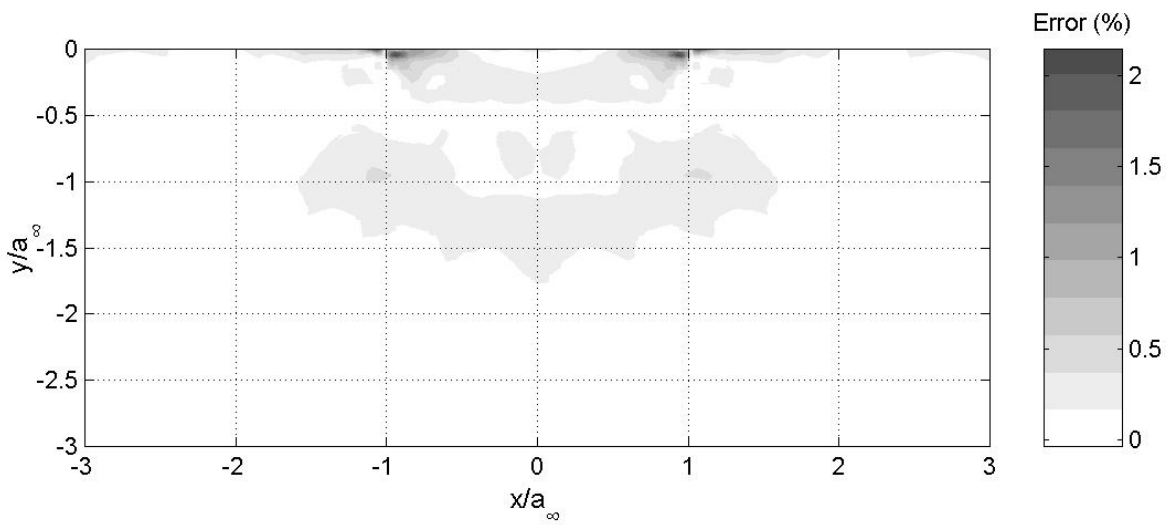


Figure 4



a)



b)

Figure 5

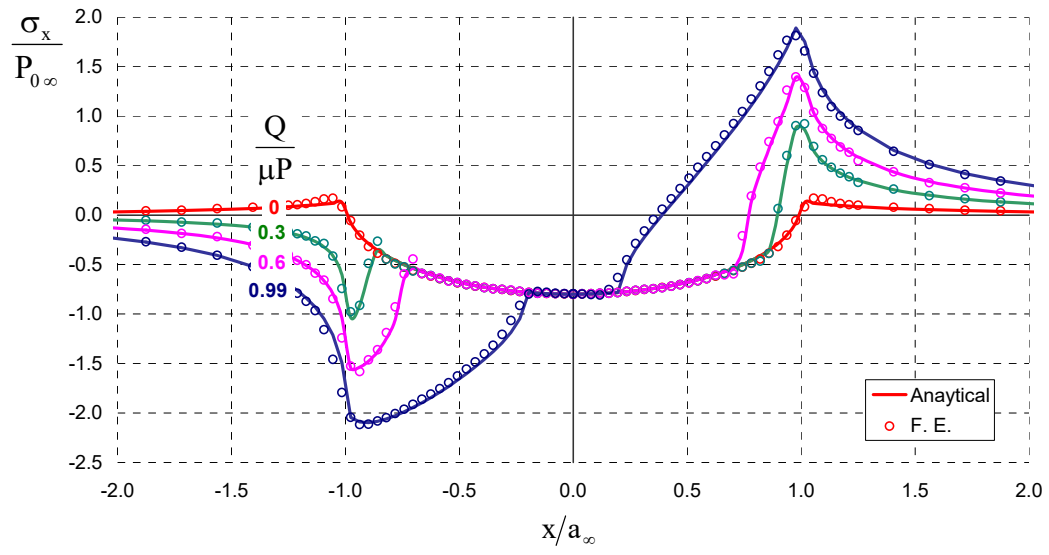


Figure 6

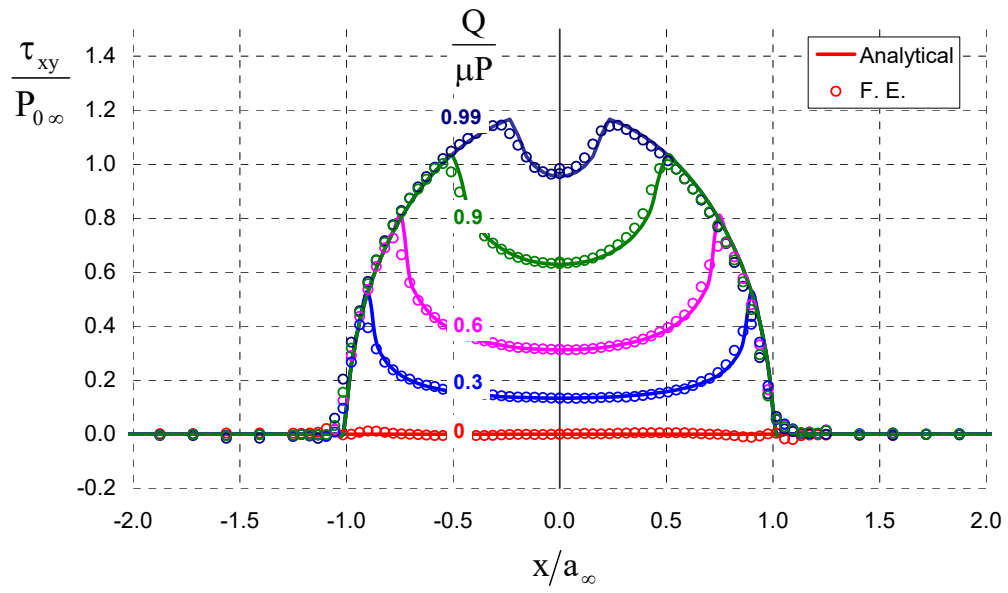


Figure 7

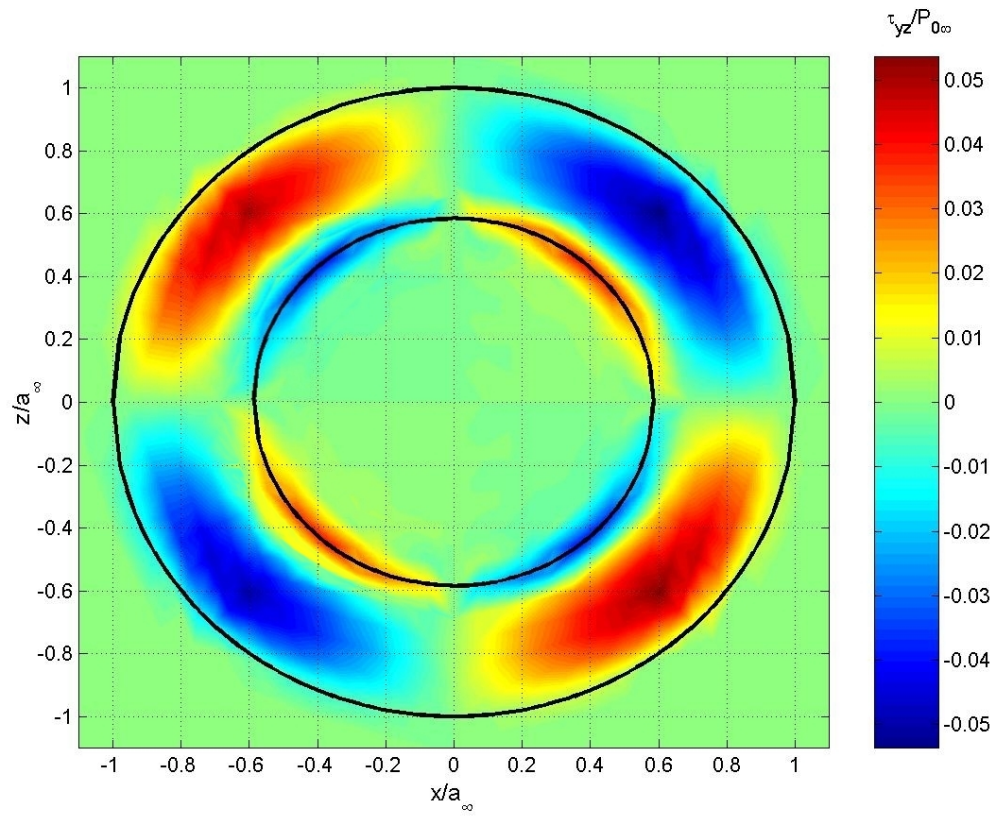


Figure 8

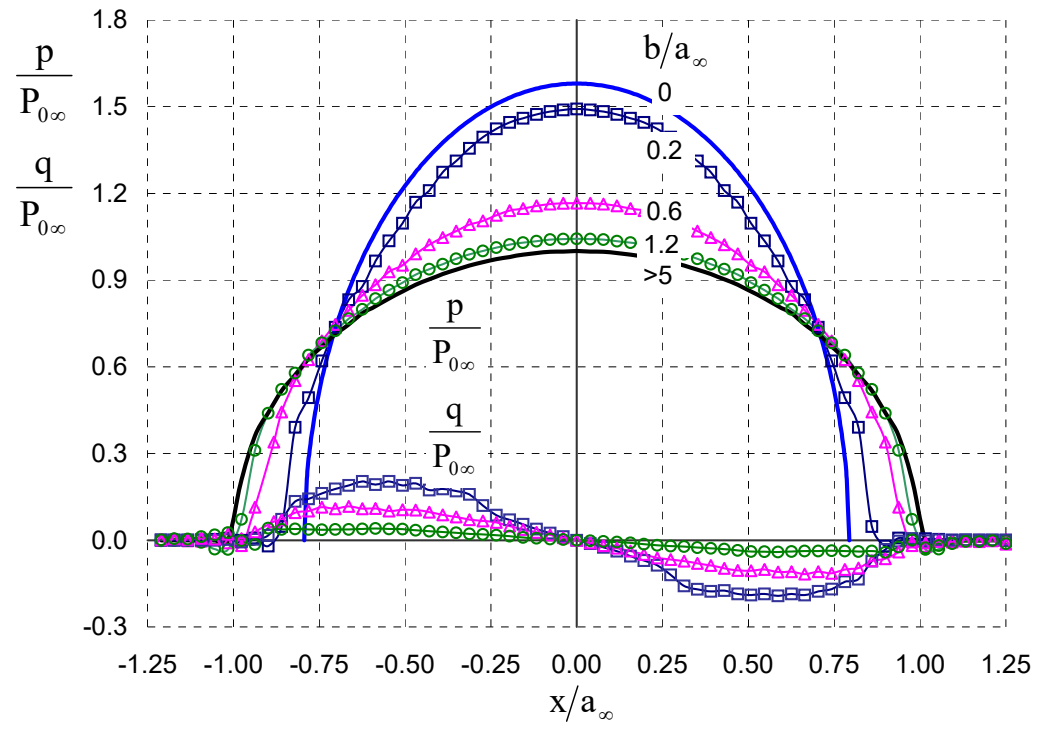


Figure 9

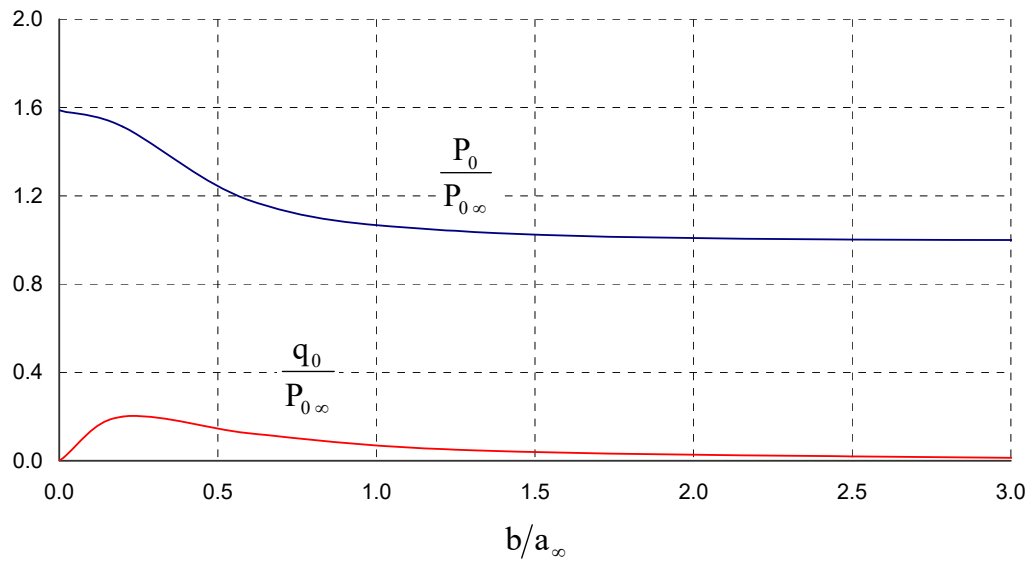


Figure 10

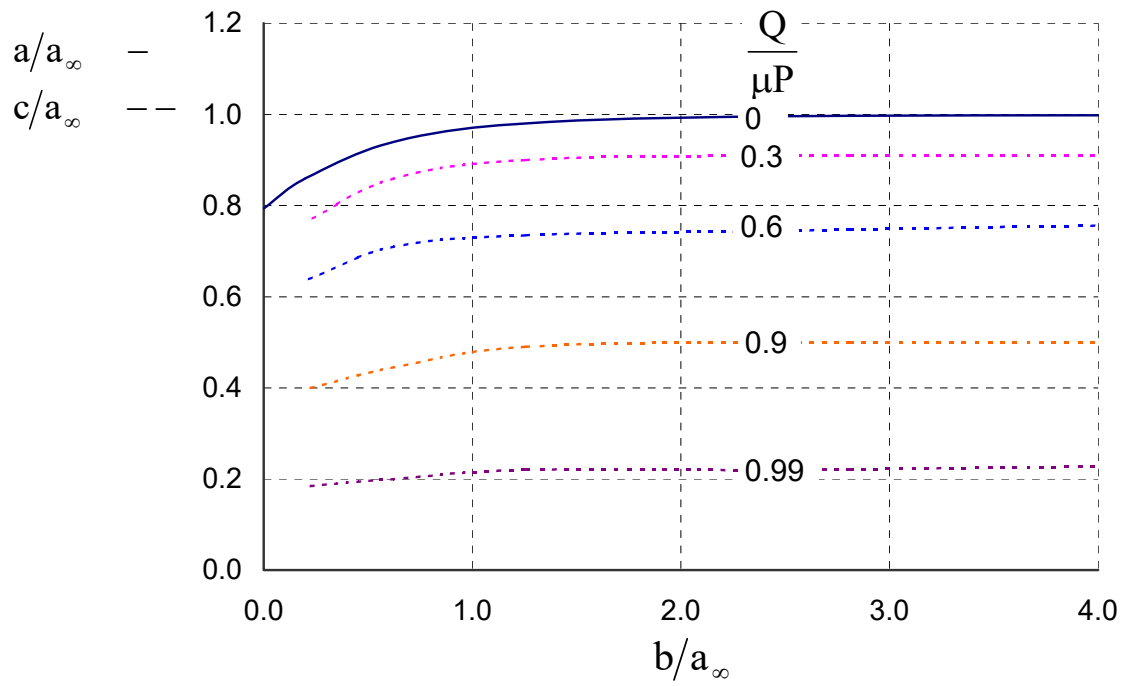


Figure 11

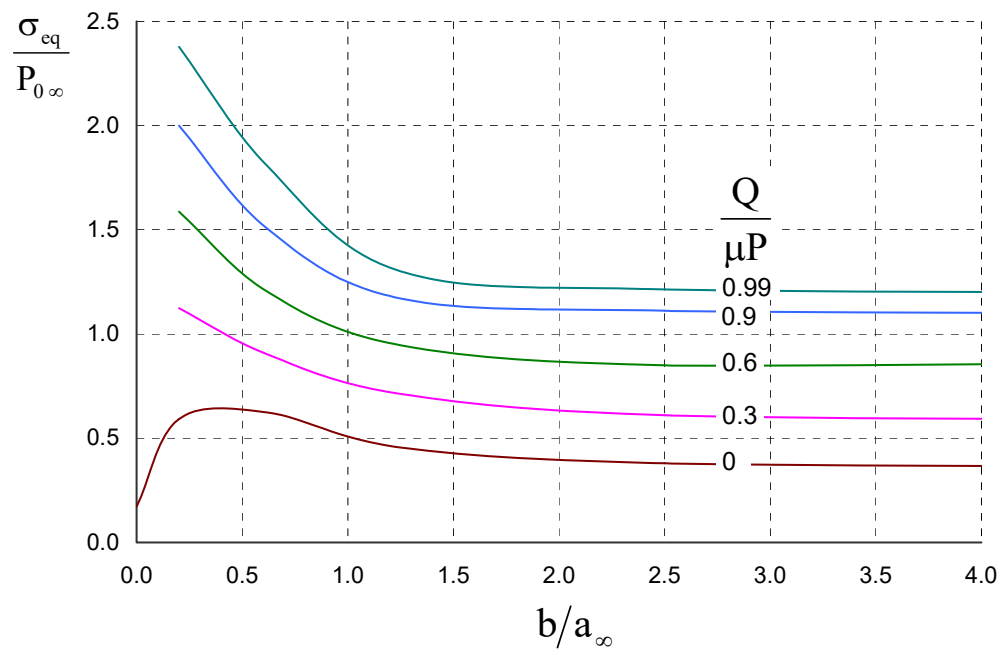


Figure 12

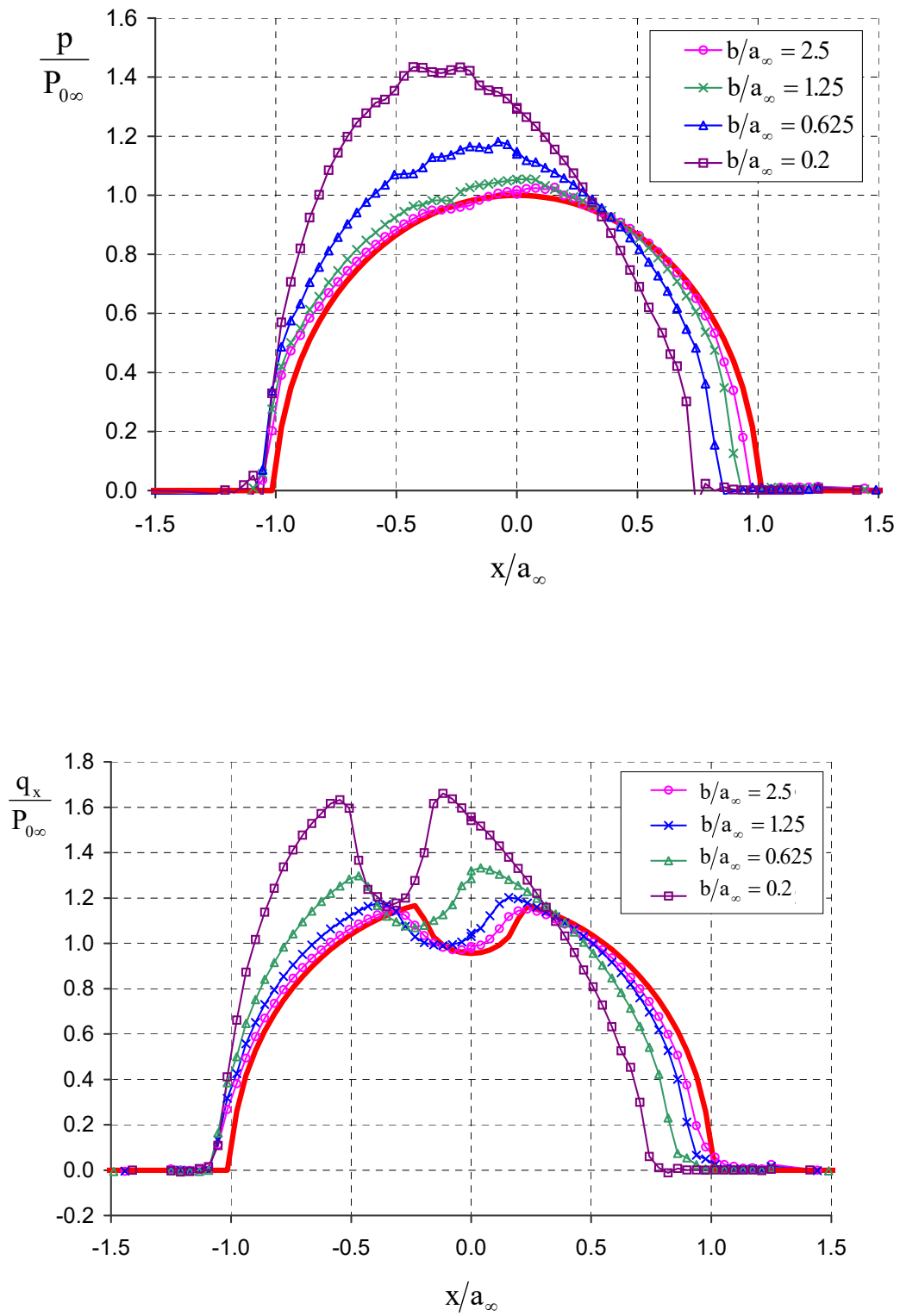


Figure 13

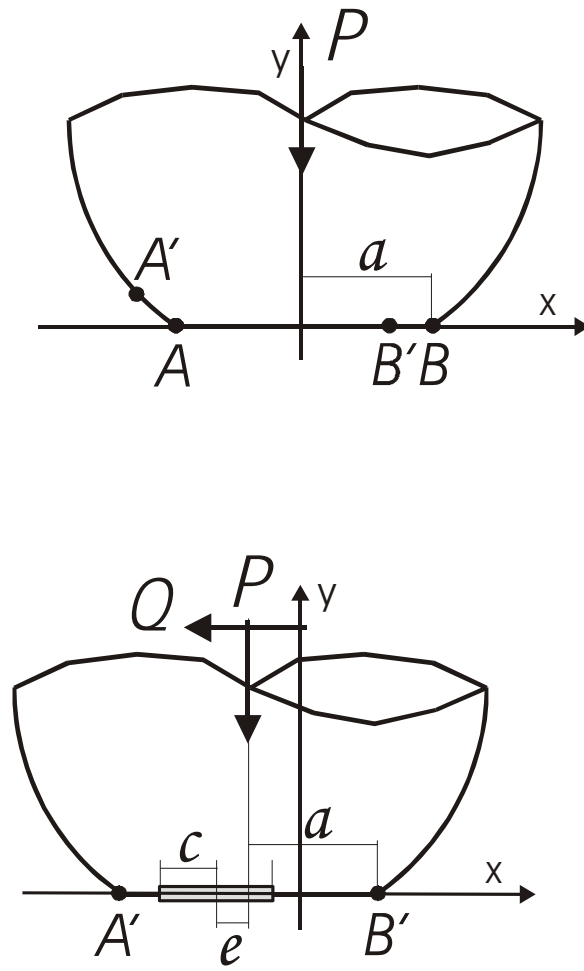
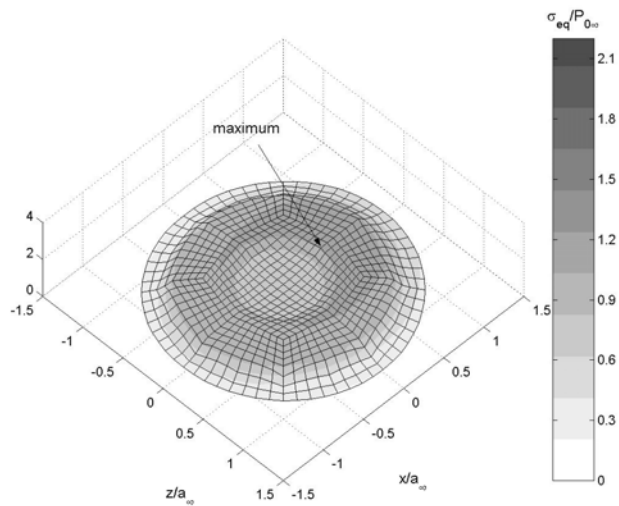
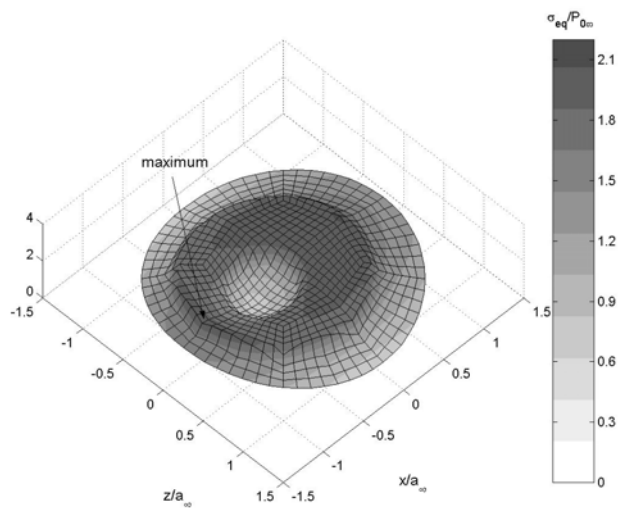


Figure 14



a)



b)

Figure 15

